Methane Source Attribution in the UK Using Multi-Year Records of CH_4 and $\delta^{13}C$

Ceres A. Woolley Maisch[1], Rebecca E. Fisher[1], James L. France[1,2], David Lowry[1], Mathias Lanoisellé[1], Thomas G. Bell[3], Grant Forster[4,5], Alistair J. Manning[6], Sylvia E. Michel[7], Alice E. Ramsden[8], Mingxi Yang[3], and Euan G. Nisbet[1]

[1]Department of Earth Sciences, Centre of Climate, Ocean and Atmosphere, Royal Holloway, University of London, Egham, UK, [2]Environmental Defense Fund, London, UK, [3]Plymouth Marine Laboratory, Plymouth, UK, [4]School of Environmental Sciences, National Centre for Atmospheric Science, Norwich Research Park, University of East Anglia, Norwich, UK, [5]School of Environmental Sciences, Centre for Ocean and Atmospheric Science, Norwich Research Park, University of East Anglia, Norwich, UK, [6]Hadley Centre, Met Office, Exeter, UK, [7]Institute of Arctic and Alpine Research, University of Colorado Boulder, Boulder, CO, USA, [8]School of Geographical Sciences, University of Bristol, Bristol, UK

Abstract Isotopic measurements of atmospheric methane are valuable for the verification of bottom-up atmospheric emissions inventories. The balance of sources in emissions inventories must be consistent with the $\delta^{13}C$-CH_4 isotopic record in the air. Long-term records of both methane mole fraction and $\delta^{13}C$ from five sites across the UK are presented, showing post-2007 growth in CH_4 and negative trend in $\delta^{13}C$, consistent with global background sites. Miller-Tans analyses of atmospheric measurements identified that the $\delta^{13}C$ signature of the methane source mix varied between -50.1 and $-56.1‰$, with less depleted $\delta^{13}C$ signatures at sites receiving air from urban areas, consistent with an increased proportion of thermogenic sources. Isotopic signatures calculated for all sites are more enriched than those expected from the bottom-up emissions inventory, suggesting that inventories for the UK either underestimate contributions of thermogenic/pyrogenic emissions or overestimate biogenic sources.

Plain Language Summary Methane is a powerful greenhouse gas. The UK has committed to net zero carbon emissions by 2050 and has signed the Global Methane Pledge, which aims to reduce methane emissions by 30% by 2030, compared to 2020 levels. This study analyses long-term measurements of methane and its carbon isotope ratio ($\delta^{13}C$) collected by Royal Holloway, University of London, across five UK sites. The $\delta^{13}C$ source signature value acts as a fingerprint, distinguishing between different sources of methane. Bulk regional isotopic source signatures for each site were calculated, showing that urban sites are dominated by thermogenic emissions (e.g., gas leaks) and rural sites by agricultural emissions (e.g., cattle). The data presented in this study are compared with data from the UK National Atmospheric Emissions Inventory (NAEI). According to the data that were collected by Royal Holloway, University of London, the NAEI underestimates the relative contribution of fossil fuel sources in the UK, such as gas from pipelines in domestic and industrial settings, or overestimates biogenic sources. This has important implications for the design of UK greenhouse gas reduction strategies.

1. Introduction

National methane emissions inventories can be verified and improved by testing for isotopic balance. Here long-term data sets from five sites across the UK are used to construct bulk regional isotopic source signatures for UK methane emissions and to test the UK's National Atmospheric Emissions Inventory (NAEI) (Tsagatakis et al., 2022).

The atmospheric methane burden has been increasing rapidly since 2006, with the strongest annual increases in the observational record in the years since 2020 (Lan et al., 2022). This growth directly challenges the hopes of the UN Paris Agreement (Nisbet et al., 2019; United Nations Environment Programme/Climate and Clean Air Coalition, 2022). Prior to 2007, methane's growth was accompanied by a sustained shift to more positive $\delta^{13}C$-CH_4 values (isotopic shift to values richer in ^{13}C), consistent with increased anthropogenic fossil fuel emissions. But from 2007, the $\delta^{13}C$ trend has reversed, and there has been a sustained trend toward more negative $\delta^{13}C$ values. The causes driving both the growth in the methane burden and the negative isotopic shift remain unclear. However, the trends are likely primarily indicative of an increasing proportion of biogenic emissions

Table 1
Longitude and Latitude of the Sites at Which RHUL Have Been Collecting Roughly Weekly Bag/Flask Samples for Atmospheric CH_4 and $\delta^{13}C$ Measurements

Site name	Latitude	Longitude	Type of sample	Collection frequency	Type of site
EGH	51.426	−0.562	Stainless steel flasks	Weekly	Suburban
BAR	56.942	−7.537	Tedlar or Flexfoil 3 L bags	Weekly	Rural/coastal
WCO L4	50.250	−4.217	Tedlar or Flexfoil 3 L bags	Weekly	Marine
WCO E1	50.033	−4.367	Tedlar or Flexfoil 3 L bags	Biweekly	Marine
WAO	52.951	1.122	Tedlar or Flexfoil 3 L bags	Weekly	Coastal

(Fujita et al., 2020; Lan et al., 2021; Nisbet et al., 2019, 2021; Oh et al., 2022; Peng et al., 2022). There may also have been a change in the oxidative capacity of the atmosphere (Nicely et al., 2018; Rigby et al., 2017; Turner et al., 2017). The United Kingdom is an "Annex 1" party to the United Nations Framework Convention on Climate Change (UNFCCC) and is thus committed to maintaining an inventory of greenhouse gas emissions. Moreover, the UK's Climate Change Act (2008) aims to achieve national net-zero carbon emissions by 2050. Additionally, the UK signed the Global Methane Pledge (2021) to reduce global methane emissions by 30% compared to 2020 levels, before 2030. Fulfilling these promises demands accurate identification and quantification of methane.

The verification of inventories allows accurate targeting of sectors for emission mitigation and reduction. Inventories are compiled by "bottom-up" aggregation, summing emissions data (e.g., from gas leaks, cattle numbers, and waste landfills). Top-down independent quantification and verification of emissions are also needed to test the inventories by directly measuring methane in the air. Long-term records at the regional scale, such as those presented in this study, are necessary for this top-down verification. Isotopic measurements are particularly powerful tools for verification as the balance of sources in emissions inventories must be consistent with the $\delta^{13}C$ isotopic record in the air (Lowry et al., 2001).

The NAEI UK inventory (Brown et al., 2022) estimates that in 2020, the leading sources of anthropogenic CH_4 emissions in the UK were agriculture, waste, energy and land use change, with emissions in kilotonnes of 997.7, 633.3, 235, and 195.3, respectively. Quantities are given to high precision, but the uncertainties in the emissions can be significant for particular sectors or gases. The NAEI estimates that in 2020, UK emissions were reduced by over half compared to 1990, in contrast to atmospheric verification results (Lunt et al., 2021; Manning, 2011). According to the NAEI, this reduction is primarily due to a reduction in landfill emissions, cessation of coal mining activity, reducing leaks in the gas distribution network, and reduced livestock numbers (Brown et al., 2022). However, these are estimates; to verify them, top-down testing of these estimates is required for both mass balance and isotopic consistency. This study aims to determine how the bulk regional isotopic source signature of methane emissions can be identified using long-term data sets from five sites across the UK and compare this to reported inventories in order to understand how the inventories can be improved.

2. Methodology

This paper analyses CH_4 mole fraction and $\delta^{13}C$-CH_4 data that have been measured by Royal Holloway, University of London (RHUL) from five locations around the UK. The samples were collected at Barra/Vatersay (BAR) in the Outer Hebrides, RHUL in Egham (EGH), Weybourne Atmospheric Observatory (WAO)—University of East Anglia, and the Western Channel Observatory (WCO) at two locations (E1 and L4) in the English Channel—Plymouth Marine Lab (PML). The collection methods involved pumping ambient air into stainless steel flasks at Egham and into Tedlar or Flexfoil bags (SKC) at the other sites. Table 1 shows the latitude and longitude of the sites (locations of sites EGH, WAO, BAR, and WCO are shown in Figure 4). The data allow for investigation of regional CH_4 and $\delta^{13}C$ trends.

The Greenhouse Gas Laboratory at RHUL has collected extensive records of methane mole fraction and stable carbon isotope ratio measurements in the UK from both mobile campaigns (Bakkaloglu et al., 2021; Levy et al., 2012; Lowry et al., 2020; Zazzeri et al., 2017) and in long-term records taken at sites across the country, presented in this paper and in Lowry et al. (2001). Table 2 shows isotopic signatures of methane sources in the UK. These values, based on the mobile campaign measurements, highlight that for UK sources, one can clearly

Table 2
Table Showing the $\delta^{13}C$ Keeling Plot Source Signatures,, for the Largest Sources of CH_4 in the UK, Collected by the RHUL Greenhouse Gas Group During UK Mobile Campaigns

SNAP category	NFR code	Source	$\delta^{13}C$ average isotopic signature UK sources (‰)	1 SD	N	Reference	Source (NAEI category)	$\delta^{13}C$ weighted by NAEI sources (‰)	1 SD	Reference
Fossil Fuels	1B1	Coal mines	−43.2	6.8	11	Zazzeri et al. (2016)	Extraction processes	−39.7	2.4	Zazzeri et al. (2017)
Fossil Fuels	1B2	Gas production and distribution	−39.3	2.6	166	Menoud et al. (2022)	Combustion (energy, commercial, industrial)	−25	3	
Agriculture	3A	Enteric fermentation	−68.6	1.8	15	Menoud et al. (2022) and Lowry et al. (2020)	Agriculture	−66.0	1.6	Zazzeri et al. (2017)
Agriculture	3B	Animal waste	−51.5	1.9	10	Menoud et al. (2022) and Lowry et al. (2020)	Biomass burning	−28	3	
Waste	5A	Landfill sites	−57.1	2.5	53	Bakkaloglu et al. (2022)				
Waste	5B	Composting and anaerobic digestion	−54.7	5.3	27	Bakkaloglu et al. (2022)	Waste	−56.3	2.1	
Waste	5C	Wastewater treatment	−52.6	3	18	Bakkaloglu et al. (2022)	Offshore (fossil fuels)	−39.7	2.4	
							Transport (road + other)	−13	5	Al-Shalan et al. (2022)

Note. The values under the column '$\delta^{13}C$ weighted by NAEI sources' are derived by mass balance using the values from references to the left, and the NAEI 2020 inventory emissions for each NFR code. These values are then used to calculate the 1×1 km grid of weighted $\delta^{13}C$ isotopic by emissions from the 2020 NAEI maps data seen in Figure 4. Note that the $\delta^{13}C$ value for gas leaks differs to that from waste and agriculture for the UK.

distinguish between gas and agriculture δ¹³C values, due to the thermogenic nature of the gas supplied to the UK, but not between waste and agriculture.

The EGH site's atmospheric data are strongly affected by local and London sources, which are highly dependent on wind direction. WAO, although coastal, is also affected by local sources, relatively clean maritime air, as well as mainland European sources and polluted UK air masses (Forster et al., 2012). In contrast, the WCO and BAR are considered less polluted sites for atmospheric measurements. These sites were chosen since they each offer different background sectors, SW-NNW for BAR, SSW-WSW for WCO and N-NNE for WAO. Data from EGH date back to 2006, BAR date back to 2011 and WAO and WCO to 2013. In October 2016 the sample location in Barra (57.029, −7.450) was moved around 11 km to Vatersay (56.942, −7.537).

Samples collected weekly at each site are sent to and analyzed at the Greenhouse Gas Laboratory, RHUL. CH_4 mole fraction is analyzed by a Picarro G1301 cavity ring-down analyzer, to the WMO X2004A scale. Stable carbon isotope ratio measurements were carried out using CF-GC-IRMS (Continuous Flow Gas Chromatography-Isotope Ratio Mass Spectrometry), according to the method outlined in Fisher et al. (2006). The reproducibility is 0.05‰ or better for most δ¹³C-CH_4 measurements. Note that for EGH, CH_4 mole fractions were measured on a HP5890 GC-FID (gas chromatograph, flame ionization detector) until 22nd March 2010, with the Picarro G1301 used thereafter.

2.1. Miller-Tans Method

Keeling (1961) introduced the idea of characterizing the isotopic value of a source by plotting δ¹³C against 1/[CH_4] which results in a *y*-intercept that represents the source signature of the data. The Keeling plot shows the relationship between the change in concentration of CH_4 and the isotopic signature, quantifying the exchange processes of carbon sinks or sources with the atmosphere. Although this method serves as an effective way of characterizing the isotopic signature of CH_4 from samples collected from the source, ideally the source should be well mixed into a consistent background airmass with no other sources interfering at the sample points (Pataki et al., 2003). This necessary constant mixing may not always be possible, especially for continuous measurement sites where the background airmass into which the source is mixed will not be constant.

A Miller-Tans plot (Miller & Tans, 2003) is an alternative method of identifying isotopic source signatures to the Keeling plot, which accounts for the possibility of a varying background. This process treats enhancements from the same source but with different background air masses as one mathematical term. Miller-Tans background values can be explicitly specified to both CO_2 or CH_4 and δ¹³C. Therefore, the Miller-Tans plot is preferred for long-term measurements or when the background air mass has changed during the measurement period of interest. The source signature ($δ_s$) is evaluated from the slope of the regression line which represents the flux-weighted average of the sources, according to the equation,

$$\delta_{obs} C_{obs} - \delta_{bg} C_{bg} = \delta_s (C_{obs} - C_{bg}) \tag{1}$$

where C refers to CO_2 or CH_4 mole fraction, δ to δ¹³C, the subscript *obs* to observed value, *bg* to background value, and *s* to source value (Miller & Tans, 2003). Miller and Tans (2003) initially used their method on CO_2 and its δ¹³C isotopes, but in the coming sections, it will be applied to CH_4.

2.1.1. Determining Background CH_4

For this work, a method of assigning background values to the mole fraction and isotope ratios, similar to that described by Miller and Tans (2003) is adopted, in which a smooth curve fit is used to simulate background values.

Miller and Tans (2003) utilize a curve fitting method presented by NOAA (Thoning & Tans, 1989). The NOAA CCGCRV program is implemented to calculate the "smooth fit" of the data, this fit is then used to identify the background values for the analysis. The smooth fit is the function fit plus the filtered residuals using the short term cutoff value (which smooths the data over 80 days). The result is a curve with only the shortest term variations removed. The method allows the user to find the function, smooth, polynomial, harmonic and trend values. The smooth curve fit allows for the seasonal variation in the parameters to be considered. Hence long-term elements in the seasonal cycle of the data are represented, which is essential for this analysis. The smooth curve fits to the data are considered by Miller and Tans (2003) to represent C_{bg} and $\delta_{bg} C_{bg}$. The smooth curve is

representative of regional averages for CO_2 or $\delta^{13}C \cdot CO_2$. See NOAA (2023) for a description of the CCGCRV program used to smooth the data and a link to the code.

The limited literature on Miller-Tans plots used for CH_4 analysis also advises using curve fits as background. One such study was carried out by Umezawa et al. (2012); they use the Miller-Tans method to study $\delta^{13}C$ and δ^2H of atmospheric CH_4 in the upper troposphere over the Western Pacific. Their study investigates different background methods; long-term trend components, best curve fits, and data collected 2 km away. Additionally, in their Miller-Tans analysis of CH_4, $\delta^{13}C$, and δ^2H in the Hudson Bay Lowlands, Canada, Fujita et al. (2018) also use a best fit curve as background and only apply Miller-Tans analysis to data that have deviated from the best fit curve by more than 3σ. Hence best fit curves will also be used in this study.

Pickers and Manning (2015) investigate and compare the NOAA CCGCRV program with other known curve fitting methods applied to atmospheric time series, HPspline and Seasonal Trend decomposition using LOESS (STL). On each of the three sites tested, CCGCRV captured the highest percentage of data points. When comparing the percentage of seasonal maxima and seasonal minima captured by the different programs for each of the five time series investigated, CCGCRV is found to capture the highest percentage of data points consistently. Since the focus is on background data in this work, it is essential for the time series to capture seasonal variation adequately. It was found that CCGCRV is affected less severely by outliers than STL. Pickers and Manning (2015) conclude that CCGCRV is the most flexible method, hence it is used in this work to calculate the smooth curve fit to use as the background values for the Miller-Tans analysis of long-term atmospheric CH_4 records collected by RHUL across the UK.

The method used by Miller and Tans (2003), where the smooth curve fit for the data collected at the site which was being analyzed was used as background values for the Miller-Tans analysis, was altered in the investigation carried out here. Due to the presence of more polluted sites in this study compared to that of Miller and Tans (2003), the smooth curve fit through a site such as EGH is not a true reflection of background values, instead the smooth curve fit through EGH data is elevated compared to background. Hence, it was decided that the smooth curve fit of data collected at Mace Head (MHD), Ireland by NOAA Global Monitoring Laboratory and measured at the Institute of Arctic and Alpine Research at the University of Colorado (Dlugokencky et al., 1994), the most appropriate background site for air reaching the UK, would be used as the background for each of the RHUL sites, instead of the smooth curve fit at each site itself. A correction has been applied to all of the RHUL $\delta^{13}C$ data, according to Umezawa et al. (2018), to account for differences in RHUL and INSTAAR isotope scales. The environmental classification type of Mace Head is Rural Background, the monitoring station is less than 100 m from the Atlantic sea shore, and 5 m above sea level, it is located at latitude 53.326444 and longitude −9.903917, around 670 km from EGH.

2.2. Method for Calculating Weighted Isotope Values From the 2020 National Atmospheric Emissions Inventory

The NAEI offers an overview of sources and trends of greenhouse gases with some records dating back to 1970 until 2 years previous to the current year (Tsagatakis et al., 2022). The data for the NAEI maps are aggregated into 1×1 km grid cells, and annual emission data are defined in units of tonnes/km^2. The emission estimates are based on a broad set of data, from those collected from individual industrial plants to those based on national energy statistics. The modeled estimates of the distribution of emissions that are provided for the NAEI maps are aggregated to corresponding United Nations Economic Commission for Europe (UNECE) sectors by using the Selected Nomenclature for Air Pollution (SNAP) sectors. SNAP reporting sectors are shown in Table 2, matched with isotopic signatures that are based on mobile campaigns carried out across several years around the UK for example, (Zazzeri et al., 2017) and are included in the database of Menoud et al. (2022). The NAEI uses a GIS environment to compile the 1×1 km resolution maps, producing a map for each sector by summing the spatially distributed proportions of the NAEI national total.

Summarizing Figures 1–4 of Tsagatakis et al. (2022), the GIS-based methodology is as follows: point sources and road transport databases are taken together with mapping distribution grids to calculate a UK national total which includes mapped point sources, mapped area sources and mapped road transport sources. These are then taken to compile air emissions and fuel use using UNECE SNAP categories—the data are split by source category and the type of fuel used, air emissions are further split by pollutant. More information on the methods used to map

emissions can be found in Section 3 of Tsagatakis et al. (2022) and the GIS methodology to compile the maps in Section 4.

Figure 4 shows a map that weights the 2020 NAEI emissions inventory by the isotopic values from Table 2. This is discussed in Section 3.3.

2.3. Numerical Atmospheric-Dispersion Modeling Methods

The Met Office's Numerical Atmospheric-dispersion Modeling Environment (NAME) is used to calculate the sensitivity of measurements, to the surrounding emissions field. This is done by releasing and tracking simulated particles backwards in time from the observation sites and establishing where they intercept the surface layer. Footprints, which refer to the sensitivity of each observation to the emissions, can then be mapped (Rigby et al., 2011). In this study, NAME III V7.2 was used with an output resolution of $0.23°$latitude $\times 0.35°$longitude. The whole study domain was $(10.7 - 79.3)°$N, $(-97.9 - 39.7)°$E. NAME was run with a UK Met Office Unified Model product for the UK, at a spatial resolution of 1.5 km and temporal resolution of 1 hr. The UK Met Office's Global Unified Model (12–17 km horizontal resolution) was used to provide meteorology for the rest of the domain at a temporal resolution of 3 hr.

In addition to this, air parcel back trajectory analysis was completed using Hybrid Single-Particle Lagrangian Integrated Trajectory model (HYSPLIT) for each of the UK sites in order to demonstrate that the airmass from BAR and PML are not commonly influenced by regions covered in the NAEI, but EGH and WAO are, see Figure S2 in Supporting Information S1. Hence, this NAME analysis was only carried out for EGH and WAO.

3. Results

3.1. CH_4 Mole Fraction and $\delta^{13}C$-CH_4 Time Series

The time series for both CH_4 mole fraction and $\delta^{13}C$ for each site can be seen in Figures 1 and 2 respectively, with the fits from the CCGCRV program applied. Due to proximity and less frequent sampling compared to other sites, WCO E1 and WCO L4 data have been combined in order to create a more comprehensive data set.

The globally averaged mole fraction of methane has increased after 2006, coupled with a shift to more depleted $\delta^{13}C$ values (Lan et al., 2022; Nisbet et al., 2016). This trend as well as the seasonal cycle in the background signal are why the Miller-Tans method is applied to this data instead of the traditional Keeling technique as the background is not constant in either CH_4 mole fraction or $\delta^{13}C$-CH_4 for this long-term data.

Figures 1 and 2 show the smooth curve and trend curve fit of CH_4 mole fraction and $\delta^{13}C$ data at MHD, collected by NOAA/INSTAAR, plotted with the RHUL data for each site. This MHD data serves as the background values for the RHUL UK sites. It can be seen that the MHD data provide a very good baseline for the RHUL data, even at the more polluted sites such as EGH, and also highlights how background air is still sometimes recorded even at this suburban site.

3.2. Miller-Tans $\delta^{13}C$ Source Signatures

In order for the Miller-Tans analysis to be carried out, the data points that form the smoothed curve of the MHD data are linearly interpolated so that their dates match those of sample dates for each RHUL site. The results from this analysis for each site can be seen in Figure 3, which includes the source signature calculated from the whole time series of each site, and Figure 4 where the values are calculated for the time period 2017–2021 for every site. This was done for comparability purposes, for each site only data from 2017 onwards was analyzed, in order for a fair comparison to WAO to be made.

The MHD NOAA/INSTAAR data is filtered according to a 3-column quality control flag, where all flagged data were removed for the purpose of this study. It is also necessary to filter the RHUL data to remove outliers such as CH_4 mole fractions which lie below the MHD background, or anomalous one off emission events (which are preferably removed here since this study is focusing on long-term regional sources, not local sources specific to the site at a specific time). Therefore, in this work the C_{obs}-C_{bg} values used in the Miller-Tans analysis were filtered by removing the top and bottom 2.5%. This resulted in the extreme 5% of values being removed, corresponding
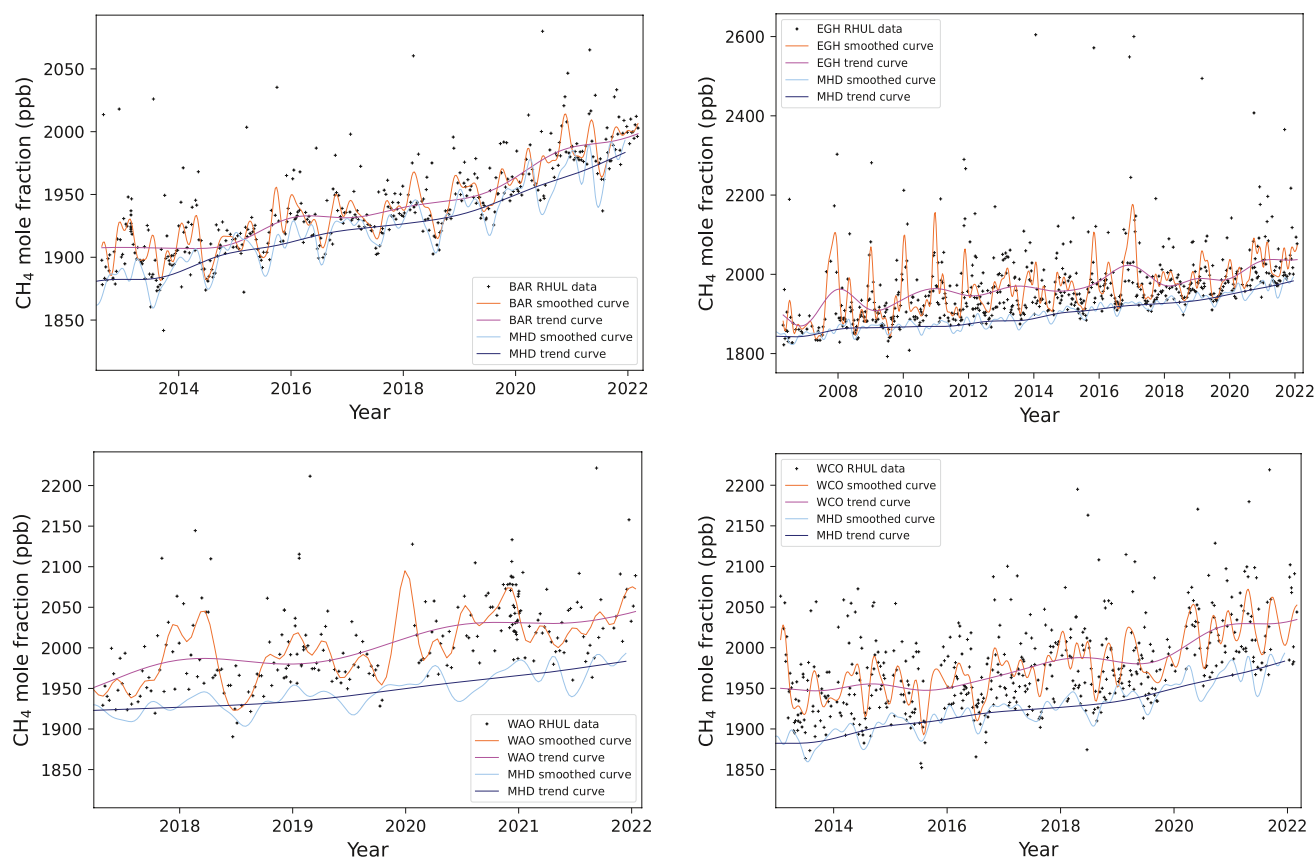
Figure 1. Times series for CH$_4$ mole fraction data measured by RHUL and collected at various sites across the UK, BAR (top left), EGH (top right), WAO (bottom left), WCO (bottom right), in bags/flasks with a temporal frequency of roughly a week. NOAA CCGCRV fitting methods, smoothed curve and trend curve, are applied as outlined in Section 2.1.1, black data points represent the RHUL data. The data here have been plotted with the smoothed curve and trend curve of the NOAA/ INSTAAR Mace Head data, in order to highlight and justify its use as background for the Miller-Tans analysis of the RHUL sites. The data from the WCO sites L1 and E4 (which lie around 26 km apart in the western English Channel) have been combined resulting in one panel to represent WCO. The data for WAO from before 2017 are removed, so that only the time period with more regular (weekly) bag sampling is represented and analyzed.

to a 95% confidence interval. The resulting Miller-Tans plots can be seen in Figure 3 (see Figure S1 in Supporting Information S1 for Miller-Tans plots that include the data that is filtered). This method is effective in filtering data points which heavily weight the regression line (and subsequently the source signature) without biasing the data. This was done so that single data points which likely correspond to one off local pollution events were prevented from heavily weighting the bulk regional isotopic source signature calculated from the slope of least squares regression line of the Miller-Tans plot.

The results of the Miller-Tans analysis for the bulk regional δ^{13}C source signatures of the RHUL UK sites are plotted on a map of weighted δ^{13}C values based on the NAEI emission maps (method discussed in Section 3.3) in Figure 4. The two data sets agree in terms of general trends between rural and more urban areas. The δ^{13}C source signatures for EGH and WAO which are often influenced by air from urban areas are more enriched than those at the rural/marine sites, WCO and BAR. This is likely due to a larger influence of thermogenic sources from more urban sites, and agricultural sources from rural sites.

3.3. Weighted δ^{13}C Values Based on Emissions From the UK Inventories

A map with data from the 2020 NAEI maps database, which has been weighted using the data in Table 2 to calculate corresponding δ^{13}C values, can be seen in Figure 4. A whole UK average δ^{13}C value based on the 2020 methane emission data set was calculated to be −58.2 ± 1.1‰. By calculating an isotopic source mix for each 1 × 1 km square, a mapped product for source mix distribution is created, which can be compared with measured sample data and highlights spatial differences in the source distribution. Comparing London emissions, there is
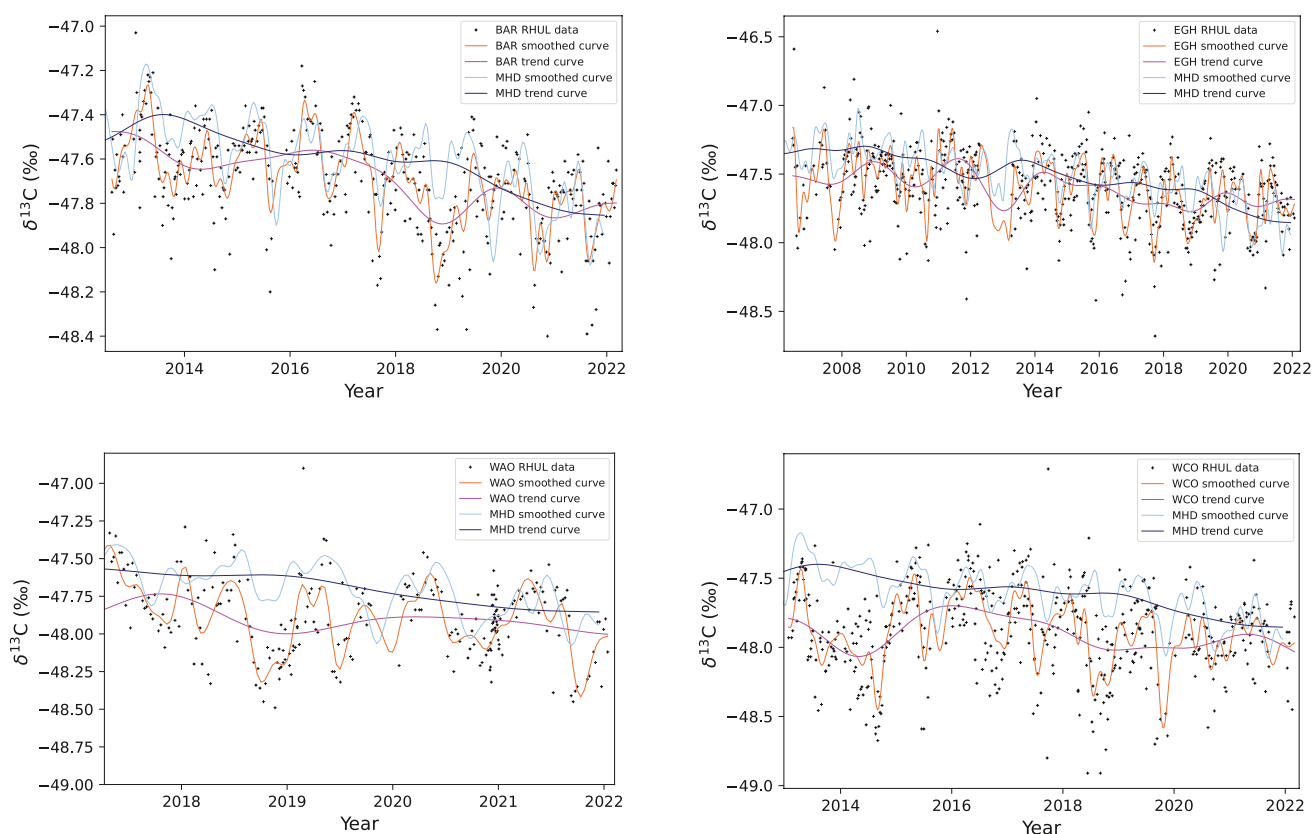
Figure 2. Times series for δ¹³C-CH₄ mole fraction data collected by RHUL from various UK sites, BAR (top left), EGH (top right), WAO (bottom left), WCO (bottom right). NOAA CCGCRV fitting methods, smoothed curve and trend curve, are applied as outlined in Section 2.1.1, black data points represent the RHUL data. The data here has been plotted with the smoothed curve and trend curve of the NOAA/INSTAAR Mace Head data, in order to highlight and justify its use as background for the Miller-Tans analysis of the RHUL sites.

more variability in measurements from surveys compared to the NAEI maps (Zazzeri et al., 2017). High emissions are seen in both rural and urban areas of the NAEI CH_4 emission maps, see NAEI (2023). Urban emissions are dominated by thermogenic sources (δ¹³C value around −40‰, see Figure 4), and rural emissions by agriculture and/or waste (δ¹³C value around −60‰). This same trend is seen in the Miller-Tans results plotted on top of the weighted map, although the derived values for the source signatures are different.

A 1,000 run Monte Carlo simulation was carried out for the weighted NAEI source signature, taking the errors presented in Table 2 into account. The resulting uncertainties for these values are one standard deviation. The error on the NAEI total is quoted as 15% (see BEIS (2023)); individual errors for each emission sector are not publicly available.

Other information on uncertainties in the NAEI maps states that the methane maps have a high uncertainty associated with them since around 44% of emissions are assigned to the agricultural sector, which has high uncertainty in its emissions. For agricultural emissions, there is a loss in data quality due to non-disclosure constraints. Data initially collected and output into 1×1 km were combined at a resolution of 5×5 km; these are then evenly distributed into 1×1 km. Similar methodology is also carried out on landfill emissions.

The Emissions Database for Global Atmospheric Research (EDGAR) (Crippa et al., 2018) offers more comparison for this work. This global database offers time series and spatial distributions of emissions of greenhouse gasses (CO_2, CH_4, N_2O) and air pollutants. The inventory utilizes IPCC methodology to provide independent emission estimates; these data are available as national totals or $0.1 \times 0.1°$ resolution global grid maps. At the time of writing, EDGARv7.0 is available, with data from 1970 up to and including 2021 released. The units of the emissions as country totals are ktonne substance/year. The data for the UK includes emissions for several sources for each year. The emissions were weighted using the same calculations as in Section 2.2 but instead of SNAP
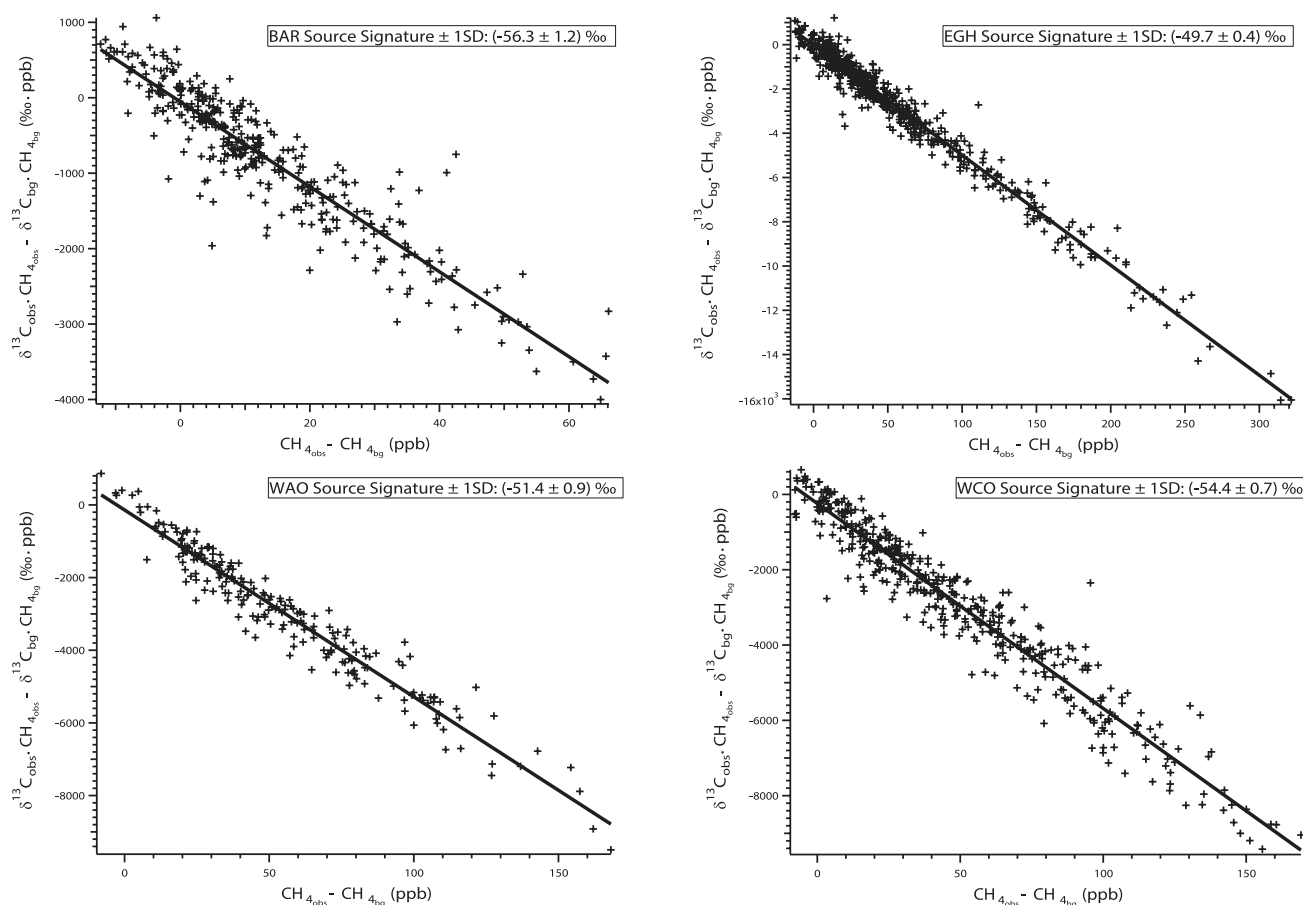
Figure 3. Miller-Tans plots for the RHUL UK sites, BAR (top left), EGH (top right), WAO (bottom left), WCO (bottom right), where the whole time series for each site has been included. Data from WCO sites E1 and L4 have been combined. The smooth curve fit of NOAA/INSTAAR data from MHD has been used for background values. Filtering has been applied here, the top and bottom 2.5% of C_{obs}-C_{bg} values from the Miller-Tans analysis were removed. The source signature is calculated from the slope of the ordinary least squares regression line. The R^2 values for BAR, EGH, WAO, and WCO are 0.81, 0.96, 0.94 and 0.94 respectively.

categories, NFR/IPCC codes and their associated source signatures were used (see Table 2 in the for codes and $\delta^{13}C$). The analysis results in a $\delta^{13}C$ value of $-61.3 \pm 1.1‰$ for the year 2021, and $-60.7 \pm 1.1‰$ for 2020 for the whole of the UK. The EDGAR source signature estimate differs from the NAEI because the two inventories have different emission estimate and activity data methods.

3.4. Numerical Atmospheric-Dispersion Modeling

The Met Office's NAME was used to calculate the sensitivity of measurements, taken at EGH and WAO, to the surrounding emissions field, shown in Figure 5. The raw NAME output files contain information about the locations of the modeled air particles at each time step. This information is processed to create hourly footprints in units of (mol/mol)/(mol/m^2/s) for each latitude/longitude grid cell. The annual mean footprint value was calculated for each latitude/longitude grid cell and converted via a Triangular Interpolation Network (TIN) interpolation so that the footprints could be mapped onto the 1×1 km NAEI emissions maps.

Then, a weighted isotopic signature, specific to WAO and EGH were calculated as follows,

$$\frac{\sum (fp \cdot emission \cdot \delta^{13}C)}{\sum (fp \cdot emission)} \qquad (2)$$

where $fp \cdot emission \cdot \delta^{13}C$ and $fp \cdot emission$ are calculated for each grid cell, and summing over all of these grid cells according to the above equation results in one weighted $\delta^{13}C$ value for WAO or EGH, where fp is the NAME
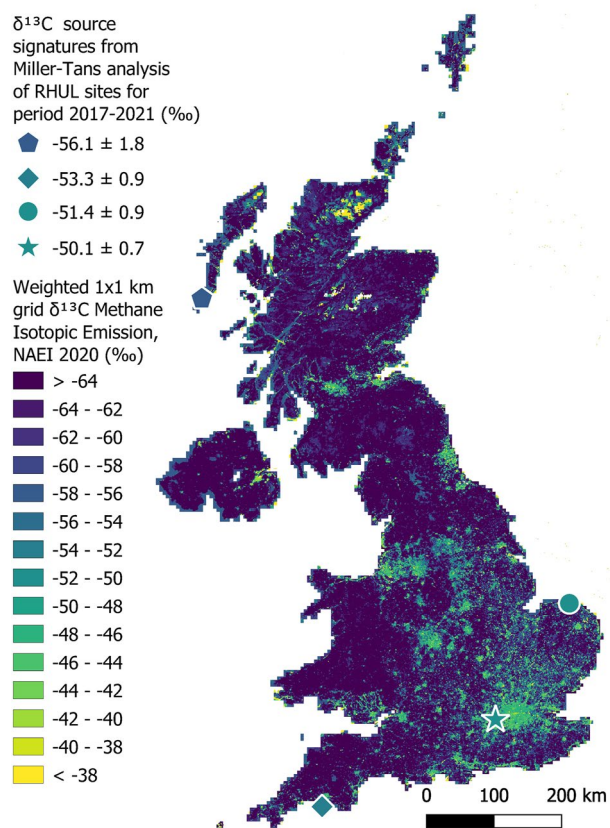
Figure 4. Bulk regional $\delta^{13}C$ source signatures calculated from RHUL long-term records at multiple UK sites. For the most robust comparison between values to be made, the period 2017–2021 is analyzed for all of the sites since the frequency of data needed for adequate Miller-Tans analysis in WAO began post-2016. Data here are filtered by removing the top and bottom 2.5% of the data for each site. BAR and WCO have more negative $\delta^{13}C$ source signatures since they are coastal background sites mainly influenced by biogenic sources. EGH has the most positive $\delta^{13}C$ value due to more industrial sources and gas leaks. WAO is frequently affected by emissions from London and mainland Europe. These values are plotted onto a 1×1 km grid of weighted $\delta^{13}C$ isotopic emission values, calculated using emission data from 2020 NAEI maps. The Other Transport and Mobile machinery sector is not included here.

footprint in units of (mol/mol)/(mol/m^2/s), emission is the NAEI maps emission in kilotonnes, and $\delta^{13}C$ in ‰ is the weighted value calculated previously in this work. This method results in a weighted NAEI/NAME source signature of -56.6 ± 1.1‰ for WAO and -54.2 ± 1.3‰ for EGH, compared with the measured source values of -51.4 ± 0.9‰ and -50.1 ± 0.7‰, respectively.

The same Monte Carlo analysis as described previously was also carried out for these source signature estimates to calculate their uncertainties since the error on NAME is assumed to be negligible. NAME has been extensively compared to other transport models and although there may still be systematic errors present, these errors are difficult to characterize for specific case studies without further comparison studies (this comparison is beyond the scope of this study).

To summarize the methodology presented in this section, the NAME footprint highlights where emissions for that site are modeled to have come from, with a sensitivity in each grid cell which represents how much of the total emission has come from this area and influenced concentrations that are recorded at the given site. This gives an area which the NAEI maps methane emission data is matched to. This results in the ability to model and calculate a source signature specific to that site, based on the emission data from the NAEI maps which is separated into sources and assigned isotopic values according to those presented in Table 2. This value is then weighted according to the NAME footprint sensitivity. This allows for a direct comparison between the inventory and the regional source signature calculated from the measurements taken at RHUL for that site.

4. Discussion

Miller-Tans analysis of all of the sites that RHUL has been collecting long-term CH$_4$ and $\delta^{13}C$ data at, show that EGH has the most enriched $\delta^{13}C$ signature (-50.1 ± 0.7)‰ of all the sites, suggesting that it is the site most affected by combustion or thermogenic sources. WAO can be affected by London and mainland European emissions (Forster et al., 2012), which is reflected in its source signature, (-51.4 ± 0.9)‰; it is not as depleted as the other coastal sites BAR (-56.1 ± 1.8)‰ and the WCO (-53.3 ± 0.9)‰ and also not as enriched as EGH. BAR and the WCO have more biogenic (agricultural) sources in the region and are coastal. Estuaries and coastal seas are also sources of CH$_4$ (Upstill-Goddard & Barnes, 2016; Yang et al., 2019). Hence, a rural to urban change in source signature is observed in this data. WCO and BAR often receive background Atlantic air, and sometimes rural air.

The general relation of urban areas corresponding to $\delta^{13}C$ values that indicate relatively more thermogenic sources than rural areas is observed in both the Miller-Tans source signatures and in the NAEI maps emissions. However, the average source signature of $\delta^{13}C$ from weighting the data from the NAEI maps for the whole UK is (-58.2 ± 1.1)‰ for 2020, even BAR, which has the most depleted source signature of the RHUL UK sites, is more enriched than the average value from the NAEI maps. These source signatures are calculated from almost 10 years of data, whereas the inventory average is based on 2020 data only, which may cause a discrepancy between the two data sets.

It should be noted that the NAEI maps data used in this study is not the same as the NAEI UK emissions data. There are differences in shipping and aviation data included in each data set (Passant, 2003), as well as wetlands, land converted for peat extraction, cropland remaining cropland, grassland and settlements remaining settlements not being included in the mapped product. This results in a difference between the CH$_4$ emissions for the NAEI and the NAEI maps of 207 kT. Had these sources been included in the maps, the weighted average calculated in this study would have been even more depleted, due to the biogenic nature of the sources that were excluded.
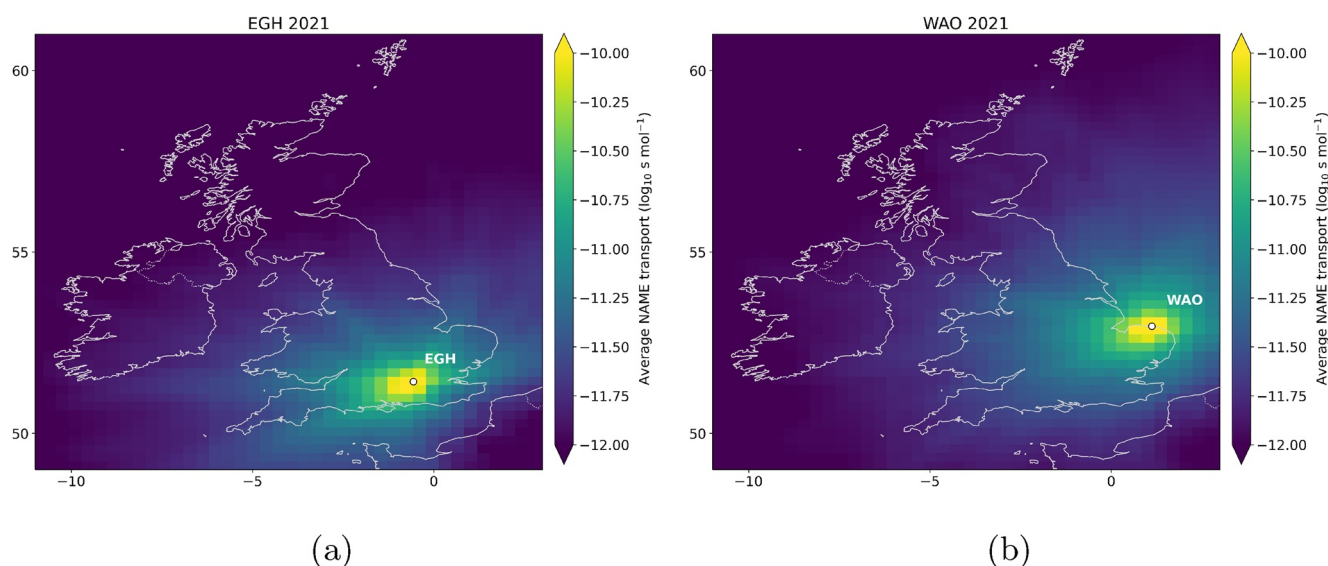
Figure 5. Maps showing the sensitivity of measurements taken at Egham (a) and Weybourne (b) for 2021 calculated by the Met Office's Numerical Atmospheric-dispersion Modeling Environment III V7.2.

This further highlights that there may be an underestimation of thermogenic sources in the NAEI maps when compared to the Miller-Tans data presented in this study.

Following from this, the weighted isotopic source signature value calculated from the EDGAR v7.0 inventory is much more depleted than those calculated from the Miller-Tans analysis of the RHUL UK sites and also that of the NAEI maps. This suggests that the same underestimation of thermogenic sources or overestimation of biogenic sources that was observed in the NAEI maps is also apparent to an even larger extent in the EDGAR inventory.

The method outlined in Section 3.4 results in a weighted NAEI/NAME source signature of $(-56.6 \pm 1.1)‰$ for WAO. This analysis was done so that a direct, site specific comparison could be made between observation and inventory. The expected observed source signature was modeled with NAEI and NAME data. This value is more depleted than the Miller-Tans value based on data from the same site, $(-51.4 \pm 0.9)‰$. This again highlights how the NAEI may be underestimating thermogenic emissions or overestimating agricultural emissions. The same calculation was done for EGH which resulted in a source signature, weighted by the NAME footprints and NAEI maps emissions, of $(-54.2 \pm 1.3)‰$. As with the WAO value, this EGH value is also more depleted than the Miller-Tans signature, $(-50.1 \pm 0.7)‰$. A difference between the regional $\delta^{13}C$ source signatures calculated from weighting the NAEI maps emissions with the NAME footprints for EGH and WAO, also observed between the Miller-Tans derived source signatures for the same two sites, demonstrates that the regional differences in source signatures between sites (likely due to higher thermogenic related emissions associated with the area in and around London) can be noticed using two distinct methods.

Recent work carried out at Imperial College London (ICL) (Saboya et al., 2022), offers a good comparison to the data collected by RHUL at EGH. The ICL measurements of CH_4 mole fraction and $\delta^{13}C$-CH_4 were taken at a latitude and longitude of 51.4999°N and −0.1749°E respectively, around 28 km east of EGH. The average $\delta^{13}C$ source signature calculated by the authors is −47.1‰, compared to those calculated in this work for EGH; $(-50.1 \pm 0.7)‰$. It should be noted that the ICL site is more likely to have a more enriched isotopic signature compared to RHUL as the site is central London, receiving urban influences air from all directions. Saboya et al. (2022) used continuous but lower precision CRDS isotope measurements from a central London site to identify the isotopic signature and compared it with inventory estimates. Signatures based on RHUL and ICL data both suggest gas dominated sources. Saboya et al. (2022) conclude that the NAEI maps underestimate gas leaks, and the same conclusions can be drawn from the RHUL Miller-Tans results presented here.

Zazzeri et al. (2023), using radiocarbon as a tracer for fossil fuel methane, also found that the fossil fraction of CH_4 in London was higher than expected in emission inventories.

Lunt et al. (2021) analyzed continuous CH_4 data recorded in the UK between 2013 and 2020, measured at 8 tall-tower sites and evaluated this data using inversion models to find the mean emissions of the UK. The aim was to evaluate the UK's methane emissions and verify national emissions. They confirmed the decline in UK CH_4 emissions from 2013 to 2020 as estimated in the NAEI. They conclude that to better constrain national and regional trends from different source sectors, and to reduce uncertainties on national emissions, more measurement sites, such as those presented here, are required.

5. Conclusions

Long-term measurements from five sites across England and Scotland, representing both urban and rural areas, have consistently shown an increase in methane mole fraction with time, coupled with a decline in $\delta^{13}C$ values, a gradient which has also been observed on the global scale (Nisbet et al., 2016). At all sites, the isotopic signature estimated from Miller-Tans plots were more enriched in ^{13}C than was expected from the NAEI or EDGAR inventories.

Using the Miller-Tans method (Miller & Tans, 2003) on the long-term data collated by Royal Holloway, University of London, it is possible to calculate bulk regional $\delta^{13}C$ source signatures. From these source signatures, a distinction between rural and urban emissions can be seen, replicating the trends observed in the NAEI mapping data set. Comparing these bulk regional signatures based on data collected by RHUL to weighted $\delta^{13}C$ values calculated using emission data from the UK's NAEI mapping data set and NAME dispersion models, it is concluded that the NAEI is underestimating the relative contribution of thermogenic/pyrogenic sources. The same can be said for the EDGARv7.0 inventory. The atmospheric top down isotope values are in better agreement with the NAEI mapping data set than EDGAR. Work on long-term measurements should continue so that reliable data can be used to create policies that will help the UK achieve its aim of net-zero carbon by 2050. This aim is more likely to be achieved if the government are able to target mitigation of identified source categories at both regional and national scales. Knowing the extent to which our environment is changing and which sources are the cause, especially with regard to the post-2006 methane increase, is vital.

Data Availability Statement

The data presented in this study including methane mole fraction and carbon isotopic values collected at five sites across the UK, as well as the Met Office NAME files for two of the sites, can be found in the following repository: Woolley Maisch, Ceres; Fisher, Rebecca; France, James; Lowry, David; Lanoiselle, Mathias; Forster, Grant; Yang, Mingxi; Bell, Tom; Ramsden, Alice; Manning, Alistair; Nisbet, Euan (2023), "Multi-year mole fraction and isotopic records for 5 UK sites," Mendeley Data, V2, https://doi.org/10.17632/phbsjtcxgx.2. The files associated with this data set are licensed under a Creative Commons Attribution 4.0 International license. The NAME transport model is available from the UK Met Office under license by contacting https://metoffice.gov.uk (Jones et al., 2007). The meteorological data used to drive the transport model from the UK Met Office operational numerical weather prediction (NWP) Unified Model (UM) are available from https://data.ceda.ac.uk/badc/ukmo-nwp (Met Office NAME Team, 2021).

References

Al-Shalan, A., Lowry, D., Fisher, R., Nisbet, E., Zazzeri, G., Al-Sarawi, M., & France, J. (2022). Methane emissions in Kuwait: Plume identification, isotopic characterization and inventory verification. *Atmospheric Environment*, *268*, 118763. https://doi.org/10.1016/j.atmosenv.2021.118763

Bakkaloglu, S., Lowry, D., Fisher, R. E., Menoud, M., Lanoisellé, M., Chen, H., et al. (2022). Stable isotopic signatures of methane from waste sources through atmospheric measurements. *Atmospheric Environment*, *276*, 119021. https://doi.org/10.1016/j.atmosenv.2022.119021

Bakkaloglu, S., Lowry, D., Fisher, R. E., France, J. L., Brunner, D., Chen, H., & Nisbet, E. G. (2021). Quantification of methane emissions from UK biogas plants. *Waste Management*, *124*, 82–93. https://doi.org/10.1016/J.WASMAN.2021.01.011

BEIS. (2023). Sector, gas, and uncertainty summary factsheets—Greenhouse gas emissions. Retrieved from https://naei.beis.gov.uk/resources/Sector_Summary_Factsheet.html#5_uncertainties

Brown, P., Cardenas, L., Choudrie, S., Del Vento, S., Karagianni, E., MacCarthy, J., et al. (2022). UK greenhouse gas inventory, 1990 to 2020 annual report for submission under the Framework convention on climate change. Retrieved from http://unfccc.int/resource/docs/2013/cop19/eng/10a03.pdf

Crippa, M., Guizzardi, D., Muntean, M., Schaaf, E., Dentener, F., Van Aardenne, J. A., et al. (2018). Gridded emissions of air pollutants for the period 1970-2012 within EDGAR v4.3.2. *Earth System Science Data*, *10*(4), 1987–2013. https://doi.org/10.5194/ESSD-10-1987-2018

Dlugokencky, E. J., Steele, L. P., Lang, P. M., & Masarie, K. A. (1994). The growth rate and distribution of atmospheric methane. *Journal of Geophysical Research*, *99*(D8), 17021–17043. https://doi.org/10.1029/94JD01245

Fisher, R., Lowry, D., Wilkin, O., Sriskantharajah, S., & Nisbet, E. G. (2006). High-precision, automated stable isotope analysis of atmospheric methane and carbon dioxide using continuous-flow isotope-ratio mass spectrometry. *Rapid Communications in Mass Spectrometry*, *20*(2), 200–208. https://doi.org/10.1002/rcm.2300

Forster, G. L., Sturges, W. T., Fleming, Z. L., Bandy, B. J., & Emeis, S. (2012). A year of H_2 measurements at Weybourne atmospheric observatory, UK. *Tellus B: Chemical and Physical Meteorology*, *64*(1), 17771. https://doi.org/10.3402/TELLUSB.V64I0.17771

Fujita, R., Morimoto, S., Maksyutov, S., Kim, H.-S., Arshinov, M., Brailsford, G., et al. (2020). Global and regional CH_4 emissions for 1995–2013 derived from atmospheric CH_4, $\delta^{13}C$-CH_4, and δD-CH_4 observations and a chemical transport model. *Journal of Geophysical Research: Atmospheres*, *125*(14), e2020JD032903. https://doi.org/10.1029/2020JD032903

Fujita, R., Morimoto, S., Umezawa, T., Ishijima, K., Patra, P. K., Worthy, D. E. J., et al. (2018). Temporal variations of the mole fraction, carbon, and hydrogen isotope ratios of atmospheric methane in the Hudson Bay Lowlands, Canada. *Journal of Geophysical Research: Atmospheres*, *123*(9), 4695–4711. https://doi.org/10.1002/2017JD027972

Jones, A., Thomson, D., Hort, M., & Devenish, B. (2007). The U.K. Met Office's next-generation atmospheric dispersion model, NAME III. In C. Borrego, & A.-L. Norman (Eds.), *Air pollution modeling and its application XVII*. (pp. 580–589).Springer.

Keeling, C. D. (1961). The concentration and isotopic abundances of carbon dioxide in rural and marine air. *Geochimica et Cosmochimica Acta*, *24*(3), 277–298. https://doi.org/10.1016/0016-7037(61)90023-0

Lan, X., Nisbet, E. G., Dlugokencky, E. J., & Michel, S. E. (2021). What do we know about the global methane budget? Results from four decades of atmospheric CH_4 observations and the way forward. *Philosophical Transactions of the Royal Society A*, *379*(2210), 20200440. https://doi.org/10.1098/RSTA.2020.0440

Lan, X., Thoning, K., & Dlugokencky, E. (2022). Trends in globally-averaged CH_4, N_2O, and SF_6 determined from NOAA global monitoring laboratory measurements. https://doi.org/10.15138/P8XG-AA10

Levy, P. E., Burden, A., Cooper, M. D., Dinsmore, K. J., Drewer, J., Evans, C., et al. (2012). Methane emissions from soils: Synthesis and analysis of a large UK data set. *Global Change Biology*, *18*(5), 1657–1669. https://doi.org/10.1111/J.1365-2486.2011.02616.X

Lowry, D., Fisher, R. E., France, J. L., Coleman, M., Lanoisellé, M., Zazzeri, G., et al. (2020). Environmental baseline monitoring for shale gas development in the UK: Identification and geochemical characterization of local source emissions of methane to atmosphere. *Science of the Total Environment*, *708*, 134600. https://doi.org/10.1016/j.scitotenv.2019.134600

Lowry, D., Holmes, C. W., Rata, N. D., O'Brien, P., & Nisbet, E. G. (2001). London methane emissions: Use of diurnal changes in concentration and $\delta^{13}C$ to identify urban sources and verify inventories. *Journal of Geophysical Research*, *106*(D7), 7427–7448. https://doi.org/10.1029/2000JD900601

Lunt, M. F., Manning, A. J., Allen, G., Arnold, T., Bauguitte, S. J., Boesch, H., et al. (2021). Atmospheric observations consistent with reported decline in the UK's methane emissions (2013–2020). *Atmospheric Chemistry and Physics*, *21*(21), 16257–16276. https://doi.org/10.5194/ACP-21-16257-2021

Manning, A. J. (2011). The challenge of estimating regional trace gas emissions from atmospheric observations. *Philosophical Transactions of the Royal Society A: Mathematical, Physical & Engineering Sciences*, *369*(1943), 1943–1954. https://doi.org/10.1098/rsta.2010.0321

Menoud, M., van der Veen, C., Lowry, D., Fernandez, J. M., Bakkaloglu, S., France, J. L., et al. (2022). New contributions of measurements in Europe to the global inventory of the stable isotopic composition of methane. *Earth System Science Data*, *14*(9), 4365–4386. https://doi.org/10.5194/essd-14-4365-2022

Miller, J. B., & Tans, P. P. (2003). Calculating isotopic fractionation from atmospheric measurements at various scales. *Tellus B: Chemical and Physical Meteorology*, *55*(2), 207–214. https://doi.org/10.3402/tellusb.v55i2.16697

NAEI. (2023). UK emissions interactive map, national atmospheric emissions inventory. Retrieved from https://naei.beis.gov.uk/emissionsapp/

Nicely, J. M., Canty, T. P., Manyin, M., Oman, L. D., Salawitch, R. J., Steenrod, S. D., et al. (2018). Changes in global tropospheric OH expected as a result of climate change over the last several decades. *Journal of Geophysical Research: Atmospheres*, *123*(18), 774–810. https://doi.org/10.1029/2018JD028388

Nisbet, E. G., Dlugokencky, E. J., Fisher, R. E., France, J. L., Lowry, D., Manning, M. R., et al. (2021). Atmospheric methane and nitrous oxide: Challenges along the path to net zero. *Philosophical Transactions of the Royal Society A*, *379*(2210), 20200457. https://doi.org/10.1098/RSTA.2020.0457

Nisbet, E. G., Dlugokencky, E. J., Manning, M. R., Lowry, D., Fisher, R. E., France, J. L., et al. (2016). Rising atmospheric methane: 2007-2014 growth and isotopic shift. *Global Biogeochemical Cycles*, *30*(9), 1356–1370. https://doi.org/10.1002/2016GB005406

Nisbet, E. G., Manning, M. R., Dlugokencky, E. J., Fisher, R. E., Lowry, D., Michel, S. E., et al. (2019). Very strong atmospheric methane growth in the 4 years 2014–2017: Implications for the Paris agreement. *Global Biogeochemical Cycles*, *33*(3), 318–342. https://doi.org/10.1029/2018GB006009

NOAA. (2023). Curve fitting methods applied to time series in NOAA/ESRL/GMD. Retrieved from https://gml.noaa.gov/ccgg/mbl/crvfit/crvfit.html

Oh, Y., Zhuang, Q., Welp, L. R., Liu, L., Lan, X., Basu, S., et al. (2022). Improved global wetland carbon isotopic signatures support post-2006 microbial methane emission increase. *Communications Earth & Environment*, *3*(1), 1–12. https://doi.org/10.1038/s43247-022-00488-5

Passant, N. R. (2003). Estimation of uncertainties in the national atmospheric emissions inventory a report produced for the department for environment, food and rural affairs; the national assembly of Wales; the Scottish executive; and the department of environment in Northern Ireland.

Pataki, D. E., Ehleringer, J. R., Flanagan, L. B., Yakir, D., Bowling, D. R., Still, C. J., et al. (2003). The application and interpretation of Keeling plots in terrestrial carbon cycle research. *Global Biogeochemical Cycles*, *17*(1). https://doi.org/10.1029/2001gb001850

Peng, S., Lin, X., Thompson, R. L., Xi, Y., Liu, G., Hauglustaine, D., et al. (2022). Wetland emission and atmospheric sink changes explain methane growth in 2020. *Nature*, *612*(7940), 477–482. https://doi.org/10.1038/s41586-022-05447-w

Pickers, P. A., & Manning, A. C. (2015). Investigating bias in the application of curve fitting programs to atmospheric time series. *Atmospheric Measurement Techniques*, *8*(3), 1469–1489. https://doi.org/10.5194/amt-8-1469-2015

Rigby, M., Manning, A. J., & Prinn, R. G. (2011). Inversion of long-lived trace gas emissions using combined Eulerian and Lagrangian chemical transport models. *Atmospheric Chemistry and Physics*, *11*(18), 9887–9898. https://doi.org/10.5194/ACP-11-9887-2011

Rigby, M., Montzka, S. A., Prinn, R. G., White, J. W., Young, D., O'Doherty, S., et al. (2017). Role of atmospheric oxidation in recent methane growth. *Proceedings of the National Academy of Sciences of the United States of America*, *114*(21), 5373–5377. https://doi.org/10.1073/PNAS.1616426114

Saboya, E., Zazzeri, G., Graven, H., Manning, A. J., & Englund Michel, S. (2022). Continuous CH_4 and $\delta^{13}C$-CH_4 measurements in London demonstrate under-reported natural gas leakage. *Atmospheric Chemistry and Physics*, *22*(5), 3595–3613. https://doi.org/10.5194/ACP-22-3595-2022

Thoning, K. W., Tans, P. P., & Komhyr, W. D. (1989). Atmospheric carbon dioxide at Mauna Loa Observatory. 2. Analysis of the NOAA GMCC data, 1974-1985. *Journal of Geophysical Research*, *94*(D6), 8549–8565. https://doi.org/10.1029/JD094iD06p08549

Tsagatakis, I., Richardson, J., Evangelides, C., Pizzolato, M., Pearson, B., Passant, N., et al. (2022). UK spatial emissions methodology: A report of the national atmospheric emission inventory 2020. Retrieved from https://naei.beis.gov.uk/reports/reports?report_id=1082

Turner, A. J., Frankenberg, C., Wennberg, P. O., & Jacob, D. J. (2017). Ambiguity in the causes for decadal trends in atmospheric methane and hydroxyl. *PNAS*, *114*(21), 5367–5372. https://doi.org/10.1073/pnas.1616020114

Umezawa, T., Brenninkmeijer, C. A. M., Röckmann, T., van der Veen, C., Tyler, S. C., Fujita, R., et al. (2018). Interlaboratory comparison of δ13C and δD measurements of atmospheric CH4 for combined use of data sets from different laboratories. *Atmospheric Measurement Techniques*, *11*(2), 1207–1231. https://doi.org/10.5194/amt-11-1207-2018

Umezawa, T., Machida, T., Aoki, S., & Nakazawa, T. (2012). Contributions of natural and anthropogenic sources to atmospheric methane variations over western Siberia estimated from its carbon and hydrogen isotopes. *Global Biogeochemical Cycles*, *26*(4). https://doi.org/10.1029/2011GB004232

United Nations Environment Programme/Climate and Clean Air Coalition. (2022). Global methane assessment: 2030 baseline report.

Upstill-Goddard, R. C., & Barnes, J. (2016). Methane emissions from UK estuaries: Re-evaluating the estuarine source of tropospheric methane from Europe. *Marine Chemistry*, *180*, 14–23. https://doi.org/10.1016/j.marchem.2016.01.010

Yang, M., Bell, T. G., Brown, I. J., Fishwick, J. R., Kitidis, V., Nightingale, P. D., et al. (2019). Insights from year-long measurements of air–water CH4 and CO2 exchange in a coastal environment. *Biogeosciences*, *16*(5), 961–978. https://doi.org/10.5194/bg-16-961-2019

Zazzeri, G., Graven, H., Xu, X., Saboya, E., Blyth, L., Manning, A. J., et al. (2023). Radiocarbon measurements reveal underestimated fossil CH4 and CO2 emissions in London. *Geophysical Research Letters*, *50*(15), e2023GL103834. https://doi.org/10.1029/2023GL103834

Zazzeri, G., Lowry, D., Fisher, R. E., France, J. L., Lanoisellé, M., Grimmond, C. S., & Nisbet, E. G. (2017). Evaluating methane inventories by isotopic analysis in the London region. *Scientific Reports*, *7*(1), 4854. https://doi.org/10.1038/s41598-017-04802-6

Zazzeri, G., Lowry, D., Fisher, R. E., France, J. L., Lanoisellé, M., Kelly, B. F., et al. (2016). Carbon isotopic signature of coal-derived methane emissions to the atmosphere: From coalification to alteration. *Atmospheric Chemistry and Physics*, *16*(21), 13669–13680. https://doi.org/10.5194/ACP-16-13669-2016